

Structural, magnetic, and critical behavior of $\text{CrTe}_{1-x}\text{Sb}_x$ Alloys

M. Kh. Hamad^{1*}, Yazan Maswadeh², E. Martinez-Teran³, A. A. El-Gendy^{3*}, and Kh. A. Ziq^{1*}

¹Department of Physics, King Fahd University of Petroleum & Minerals, Dhahran 31261, Saudi Arabia

²Department of Physics and Science of Advanced Materials Program, Central Michigan University, Mt. Pleasant, Michigan 48859, USA.

³Department of Physics, University of Texas at El Paso, TX79968, USA

Abstract

We investigate the structural and critical properties of $\text{CrTe}_{1-x}\text{Sb}_x$ with $0.0 \leq x \leq 0.2$. The XRD patterns revealed that Sb-substitution resulted in a pure *NiAs*-hexagonal structure with $\text{P6}_3/\text{mmc}$ (194) space-group. Lattice refinement of the structure revealed little changes in the *a*-lattice parameter, along with a more pronounced reduction in the *c*-axis. The critical behavior in $\text{CrTe}_{1-x}\text{Sb}_x$ has been investigated using the magnetization isotherms near the ferromagnetic transition. The obtained critical exponents (β , γ , and δ) revealed that all samples (with $0.0 \leq x \leq 0.2$) closely follow a mean field-like behavior with ferromagnetic Curie temperature (T_c) near room temperature. The results from Widom scaling relation indicating self-consistency of the acquired values. Moreover, the magnetization isotherms near the Curie temperature follow a universal scaling behavior, giving further support for the obtained critical exponents.

Key words: Critical behavior, Critical exponents, Universal scaling behavior.

*Corresponding authors: mhamad@kfupm.edu.sa; aelgendy@utep.edu; kaziq@kfupm.edu.sa

1- Introduction

Cr-based pnictogens and chalcogens continue to attract the attention of scientists due to their versatile physical properties [1-5]. These properties range from superconducting to semiconducting and half-metallic [6-7], ferromagnetic van der Waals to antiferromagnetic (AFM) behavior [8-14]. Some of the emerging possible applications are in magnetic cooling and spintronic devices [14]. The binary compounds of Cr-pnictogens (N, As, Sb) and the Cr-chalcogens (S, Se, Te) crystalize in the hexagonal *NiAs* crystal structure [1-5], however the

chemical bonding may lead to diverse magnetic and physical properties. Ionic bonding dominates the chalcogenides, while the bonding in pnictide is non-ionic. For instance, Cr_xTe is a ferromagnetic (FM) material with a Curie temperature covering wide range (320 – 360 K) depending on the value of x [6-15]. It is well established that Cr_xTe is non-stoichiometric and does not occur in pure-hexagonal phase [16-18]. While substitution at the Cr sites helps to stabilize the hexagonal NiAs structure. Deficiency and defects may also stabilize other structures like trigonal Cr_2Te_3 and monoclinic Cr_3Te_4 structure. Chromium antimony CrSb is antiferromagnetic with $T_N \sim 700\text{K}$, it crystallizes in a NiAs-type structure [19-23] with $\mu_{\text{eff}} = 3.89 \mu_B$ [24, 25]. In CrSb; the Cr spins are aligned ferromagnetically within the basal plane; while in the adjacent planes the spins are aligned antiferromagnetically [23]. Substitution in the solid solutions of $\text{CrTe}_{1-x}\text{Sb}_x$ affects the spins configurations and the magnetic phase in this compound [22, 26]. Increasing the Sb-concentrations; in $\text{CrTe}_{1-x}\text{Sb}_x$ leads to a gradual reduction in FM ordering temperature and the saturated magnetization along with moderate reduction in unit cell volume. At high concentration of Sb, a more complex magnetic phases may occur such as canted spin structures, noncollinear spin configurations and even spin-glass like behavior have been observed [14, 27-28]. Some of these magnetic changes qualitatively agree with de Gennes model of the double exchange interaction in AFM-FM system [29].

Preliminary critical behavior analysis in $\text{CrTe}_{1-x}\text{Sb}_x$ has been published in an earlier work [30] where we investigate the effect of Sb substitution over relatively wide range. The modified Arrott plots and Kouvel–Fisher critical exponents’ analyses revealed that upon increasing the Sb, the critical exponents deviate significantly from the mean field values and gradually shifts towards 3D Heisenberg models. More recently, we found that repeated grinding and annealing during sample preparation improves the phase purity in $\text{CrTe}_{1-x}\text{Sb}_x$ especially at low Sb-concentration [14]. For

these samples, we investigated the magnetocaloric effect near room temperature $\text{CrTe}_{1-x}\text{Sb}_x$ and found that the relative cooling power is comparable to pure Gd- the prototype magnetocaloric material.

In this work, we extend our investigation of the magnetic and the structural properties of $\text{CrTe}_{1-x}\text{Sb}_x$ alloys at low Sb concentrations. The samples used in this study are the same samples we used in Ref. 14. We also investigate the detailed properties of the critical behavior near the FM-PM transition in these newly prepared samples and compare them with our earlier works [30]. We also include evidences on the changes in the bond length and angle with Sb-substitution that ultimately may affect the magnetic and critical behavior. This may lead to a better understanding of the observed differences with earlier work on the critical behavior [30] in this material.

2- Experimental Techniques

Polycrystalline $\text{CrTe}_{1-x}\text{Sb}_x$ ($x \leq 0.2$) were prepared using high temperature solid-state reaction [31-32]. High purity (4-5N) powders of Cr, Te, and Sb are used. The detail of the preparation method is reported in our previous work [30]; however, for the samples in this study we used several repetition of intermediate grinding and annealing to improve the phase purity and quality of the samples. Bruker X-ray diffractometer D2-Phaser with Cu $K\alpha$ ($\lambda=1.54056 \text{ \AA}$) has been used to obtain the powdered XRD patterns over $20\text{-}80^\circ$ [14, 33]. We used Rietveld refinements available in FULLPROF software to analyze the XRD patterns. Quantum design 3-Tesla VersaLab has been used to collect the magnetic data in the temperature range of 50-400K.

3- Analysis and Results

Figure 1 shows the room temperature XRD patterns of the studied $\text{CrTe}_{1-x}\text{Sb}_x$ samples. Rietveld refinement of the data was carried out to determine the lattice parameters, phase purity, and

structure [34, 35]. The results and the lattice parameters for all investigated samples are discussed in details elsewhere [14]. Those observations are consistent with the noticed shifts of the positions of the diffractions peaks with the increasing the Sb substitution ration in the samples (Fig. 2.), the color-map at Figure 2 shows a noticeable shift in the $(0\ 0\ l)$ peaks to higher angles indicating a shortening in the c -lattice parameter in direct space.

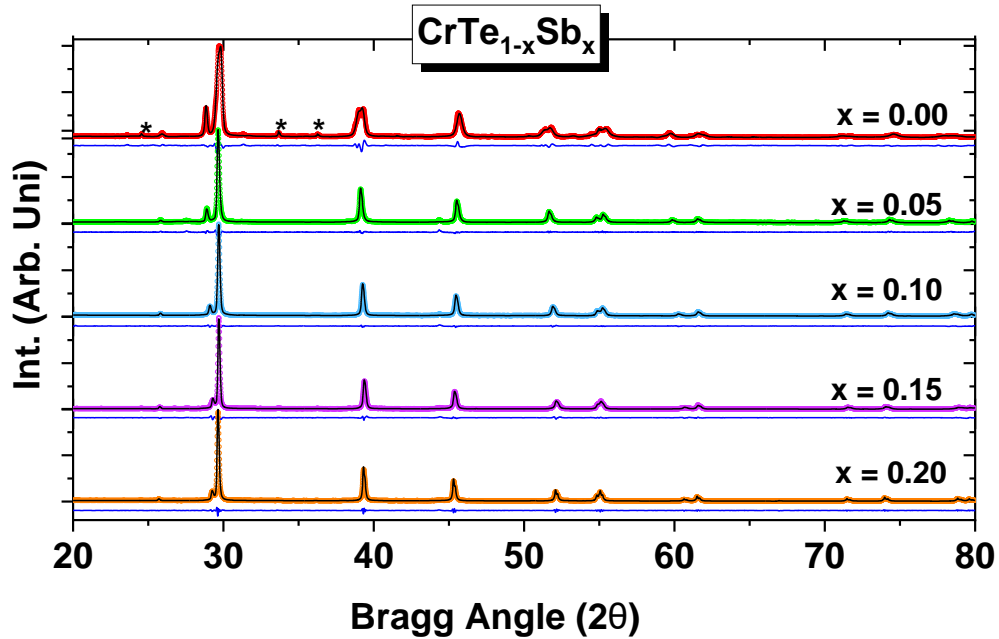


Figure 1: XRD patterns for $CrTe_{1-x}Sb_x$. The stars indicate the position of the impurity phase.

A relatively smaller shift to the left in the $(h\ k\ 0)$ peaks, that indicates a relaxation along the basal plane a -lattice. Moreover, the figure (for $x=0.0$) also reveals the presence of secondary-phase Cr_2O_3 , which has a trigonal structure with R-3c space group, leading to the nonstoichiometric Cr_xTe sample in line with earlier results [8]. *Street et al.*, concluded that Chromium-telluride Cr_xTe exists over a range of Te-concentration with the hexagonal structure [8, 36]. The Wyckoff positions for the hexagonal structure are given in Table 1. Sb-substitution causes relaxation of the

atomic-bond along (a - b) axes, this probably will be reflected residual stress along the c -axis (Fig. 3) leading to the observed variations in the lattice parameters and the overall increase in the volume of the unit cell for $x=0$ - 0.10 [see 14].

Table 1: The Wyckoff position for $\text{CrTe}_{1-x}\text{Sb}_x$ hexagonal structure space group $P6_3/mmc$ (194).

Atom	Wyckoff	Site	x/a	y/b	z/c
Cr	2a	-3m.	0	0	0
Te/Sb	2c	-6m2	1/3	2/3	1/4

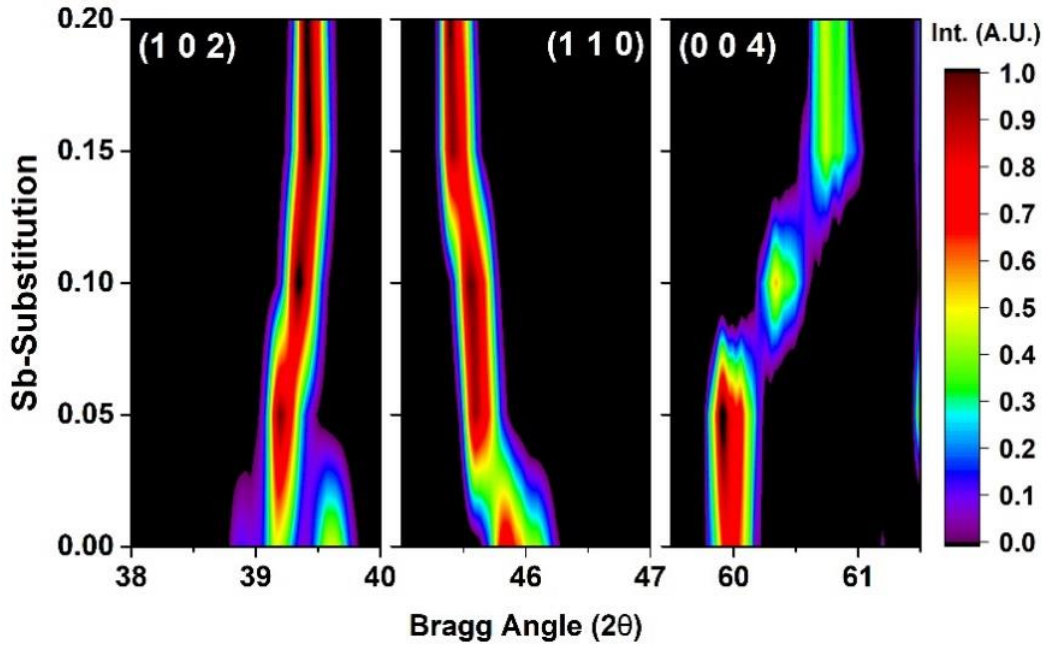


Figure 2: A colorful map of selected diffraction peaks with Miller indices shows the changes in peaks position a long with increasing the Sb substitution ratio in the $\text{CrTe}_{1-x}\text{Sb}_x$ samples, the intensity of the peaks increases by going from violet to dark red color. The y-axis increases along with the Sb concentration.

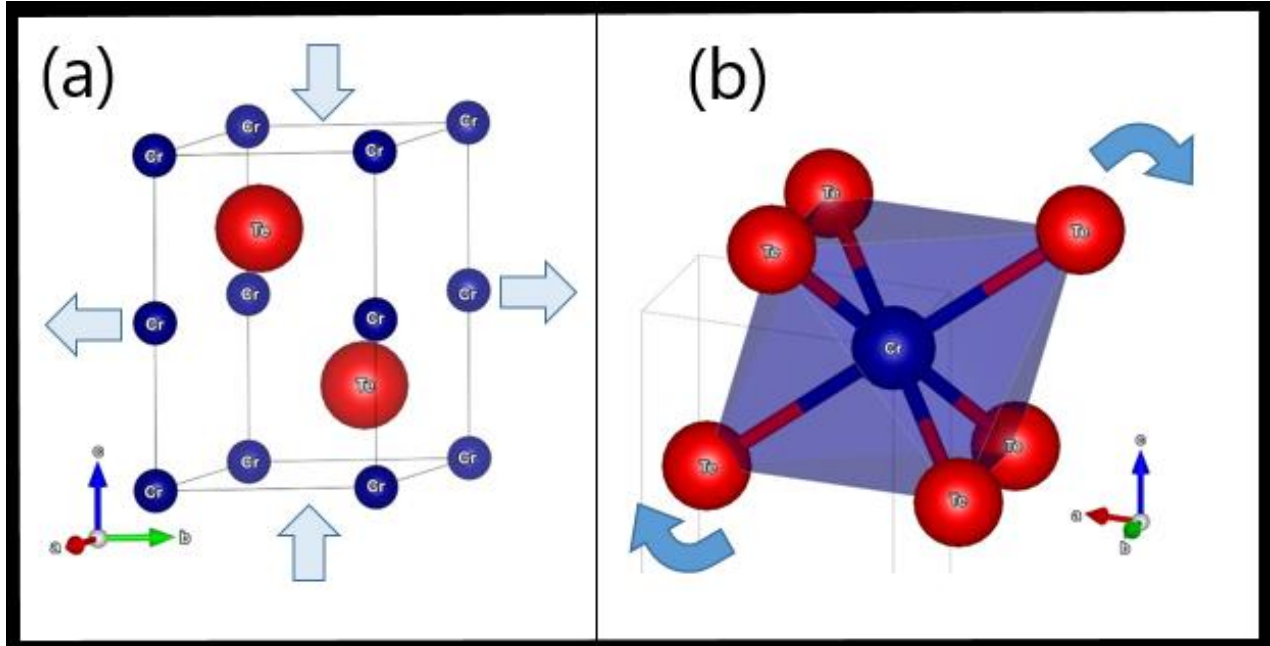


Figure 3: The unit cell structure of the $\text{CrTe}_{1-x}\text{Sb}_x$ hexagonal phase. The red balls (big) represent Te atoms, while the blue ones (small) represent Cr atoms. the arrows at (a) indicates the changes in the unit cell dimensions by increasing the Sb substitution ratio, (b) shows the CrTe octahedron.

The magnetization dependence on temperature in the range of 50-400 K at $H=0.03\text{Tesla}$ is published elsewhere [14]. The thermomagnetic curves for the selected samples ($x = 0.00, 0.10,$ and 0.20) reveals a clear FM-PM phase transition at an inflection points $\sim 325.0, 296.0,$ and 287.0 K respectively [14]. The results also reveal a slight increase in the magnetization along with sharper transition increasing the concentration of antimony. This probably indicates an increase in the effective magnetic moment per Cr-ion resulting from the exchange interaction with increasing Sb concentration. Fig. 4 presents the variations of the inverse magnetic susceptibility (χ^{-1}) with temperature. In the paramagnetic region (i.e above T_c), the inverse magnetic susceptibility obey Curie-Weiss law $\chi = C(T - \theta_p)^{-1}$, where C and θ_p are the Curie constant and the Curie temperature respectively, following a linear behavior down to θ_p in all samples. The linear extrapolation gives the following (θ_p) values 344, 309, and 302 K for $x=0.0, 0.1$ and 0.2

respectively [14]. The values of θ_p are higher than the Tc values obtained from the inflection points of the M vs. T curves. This probably suggests more complex spin configuration than normal FM spin configuration. Recently *Kong et al* observed similar results in CrSbSe₃ [37].

The linear portion of the χ^{-1} vs. T curves can be used to evaluate the effective magnetic moment μ_{eff} using $\mu_{eff} = \sqrt{3k_B C/N} = \sqrt{8C} \mu_B$, where C is the inverse of the slope and μ_B is the Bohr magneton. The obtained values are $3.92\mu_B$, 4.40 and 4.56 for x=0.0, 0.1 and 0.2 respectively. The expected value for Cr^{3+} is $3.87\mu_B$ [24, 25]. These values indicate a gradual increase in the Cr-effective moment with increasing Sb concentration. These values are in line with the noticed increase in the observed magnetization seen in [14]. The obtained values of μ_{eff} along with θ_p are listed in Table 2.

Table 2: The effective magnetic moments and θ_p values for the CrTe_{1-x}Sb_x.

	x=0.00	x=0.10	x=0.20
θ_p (K)	342.(9)	308.(3)	301.(0)
μ_{eff} (μ_B)	3.9(2)	4.4(0)	4.5(6)

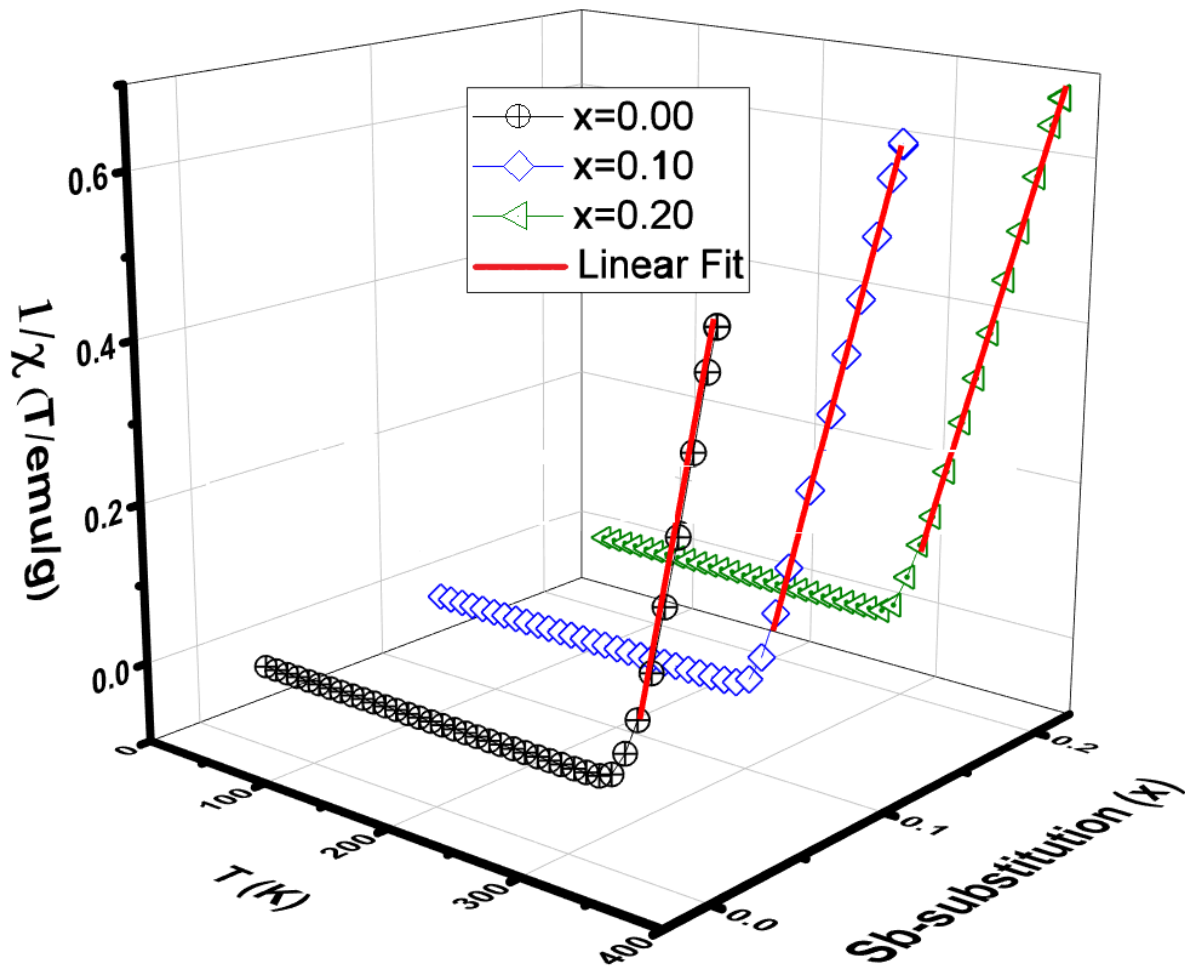


Figure 4: Temperature-dependent inverse magnetization for different $\text{CrTe}_{1-x}\text{Sb}_x$ samples measured at $H=0.03$ T.

The magnetic isotherms $M(H, T)$ of CrTe sample are shown in figure 5 in the temperature range of 300-376 K. The magnetic behavior in Fig. 5 is deeply discussed elsewhere [14]. The magnetization data in Fig. 5 are presented in modified Arrott-plots (MAP) in Fig. 6 in order to investigate the critical behavior and other magnetic properties in the following sections [13, 38-39].

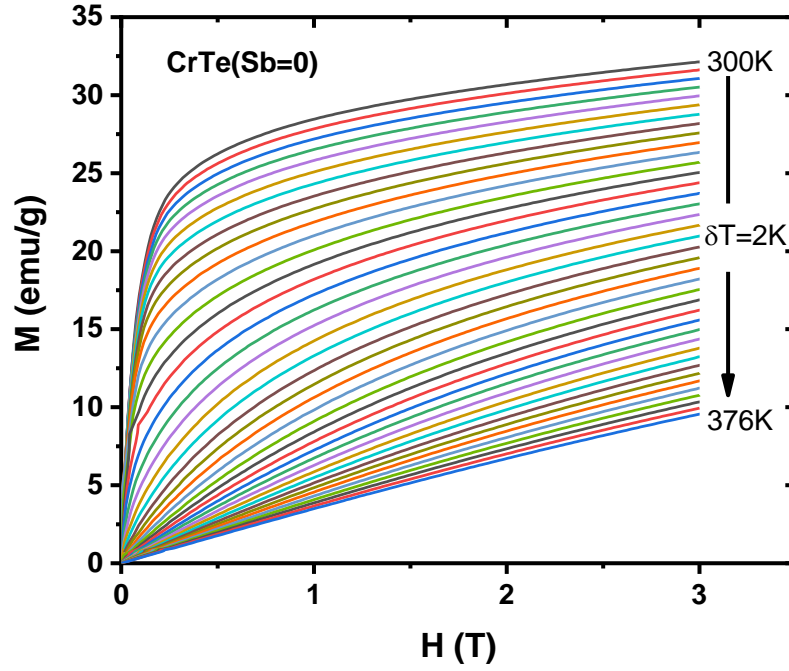


Figure 5: Variations of the magnetization with field with $\Delta T=2K$ intervals for CrTe sample.

4- Critical behaviors

The modified Arrott-plots (MAP) of the magnetization along with Kouvel-Fischer (*K-F*) plots greatly refines the critical exponents near the phase transition [40-41]. The K-F analysis is based on obtaining a linear behavior of the inverse the magnetic susceptibility (χ_0^{-1}) and the spontaneous magnetization (M_s). Moreover; M_s and χ_0^{-1} linear graphs follows a universal behavior and their slopes determine the critical exponents [42]. M_s and χ_0^{-1} can be obtained from:

$$M_s(T) = M_0(-\epsilon)^\beta, \quad \text{below } T_c \quad (1)$$

$$\chi_0^{-1} = (h_0/m_0)\epsilon^\gamma, \quad \text{above } T_c \quad (2)$$

$$M = DH^{1/\delta}, \quad \text{at } T_c \quad (3)$$

Where β , γ , and δ are the critical exponents; ϵ is the reduced temperature; D , M_0 and h_0/m_0 are the critical amplitudes and M is the critical isotherm $M(H)$ at T_c [43]. The critical exponents β, γ take different values in different magnetic models.

According to the MAP analysis, the magnetic isotherms at high fields are expected to be parallel lines for the correct set of critical exponents. The analysis is based on Arrott-Noakes equation of state; namely:

$$(H/M)^{1/\gamma} = (T - T_c)/A + (M/B)^{1/\beta} \quad (4)$$

where, A and B are constants [44].

The commonly used magnetic models are: the tricritical mean-field ($\beta = 0.25$; $\gamma = 1$), 3D-Heisenberg ($\beta = 0.365$; $\gamma = 1.336$) and the 3D-Ising ($\beta = 0.325$; $\gamma = 1.24$) [44].

In figure 6 we present the variation of $M^{1/\beta}$ with $(H/M)^{1/\gamma}$ for $CrTe$ sample using various magnetic models. The initial slopes of the curves in Fig 6 are positive above and below T_c , according to Banerjee; the positive slopes indicate a second-order phase transition [45]. The slopes at high fields in figure 6 can be used to obtain the relative slope (RS) analysis that allows us to determine the most suitable magnetic model that closely represents the magnetic isotherms. The RS values obtained from Fig 6 are represented in Fig. 7. The RS curve obtained from mean-field model is the closest to the horizontal line at $RS = 1$ above and below T_c indicating that the mean field model closely represents $CrTe$ magnetic state [46]. Similar analysis has been applied for $CrTe_{1-x}Sb_x$ samples. We found that the mean field model is closely represents the magnetic isotherms in the modified Arrott plot representation. The RS curves for $CrTe_{1-x}Sb_x$ samples are presented in Fig. 7 and the modified Arrott plots using the mean field theory (MFT) (for $x=0.10$ and 0.20) are shown in Fig. 8. It is worth mentioning that, for $x=0.20$, there are noticeable differences between the previously published data and results obtained in this work (see [30] for comparison). Such

differences may be caused by the better quality of the samples used in the current study and the observed relaxation of the atomic-bond in the $(a-b)$ -plane especially at high Sb-concentration.

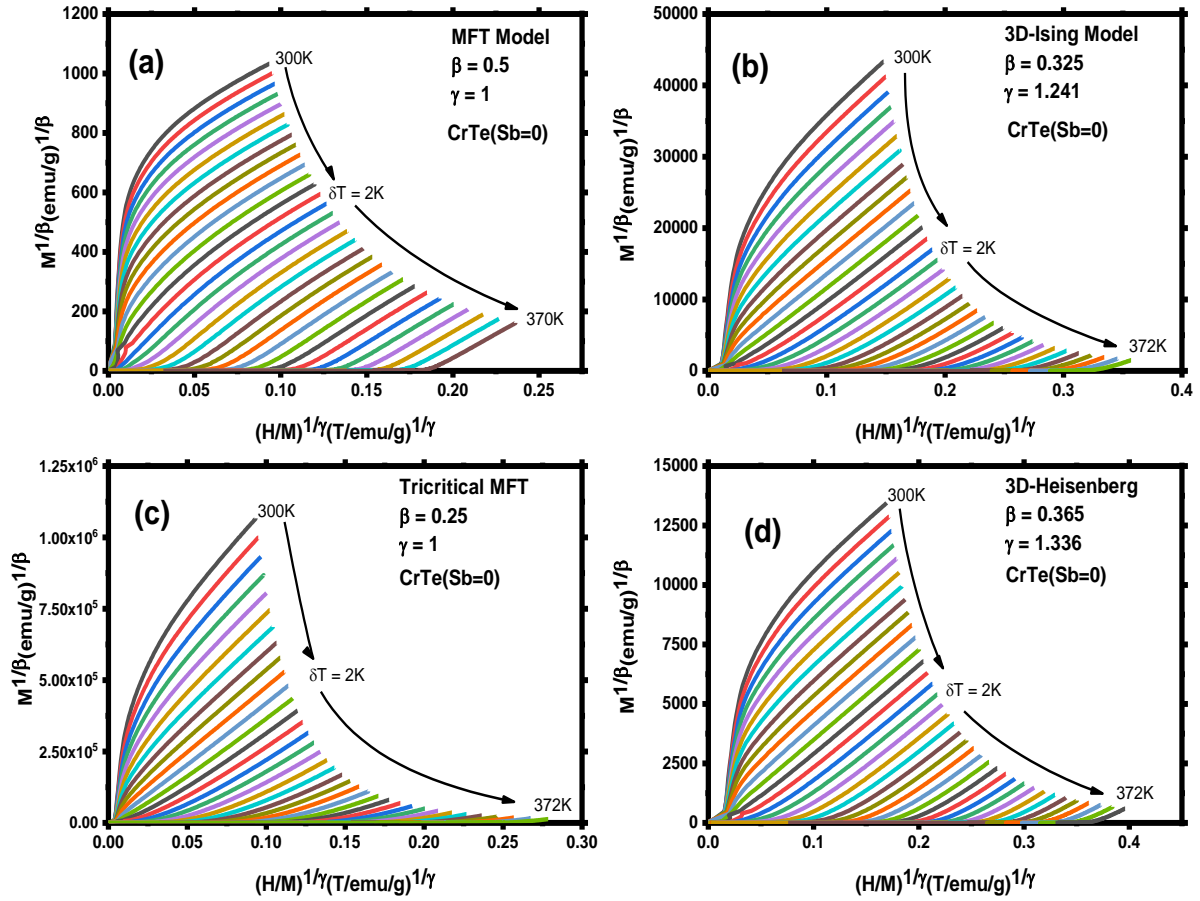


Figure 6: Modified Arrott-plots for CrTe: (a) Mean-Field. (b) 3D-Ising. (c) Tricritical mean field and (d) 3D-Heisenberg model.

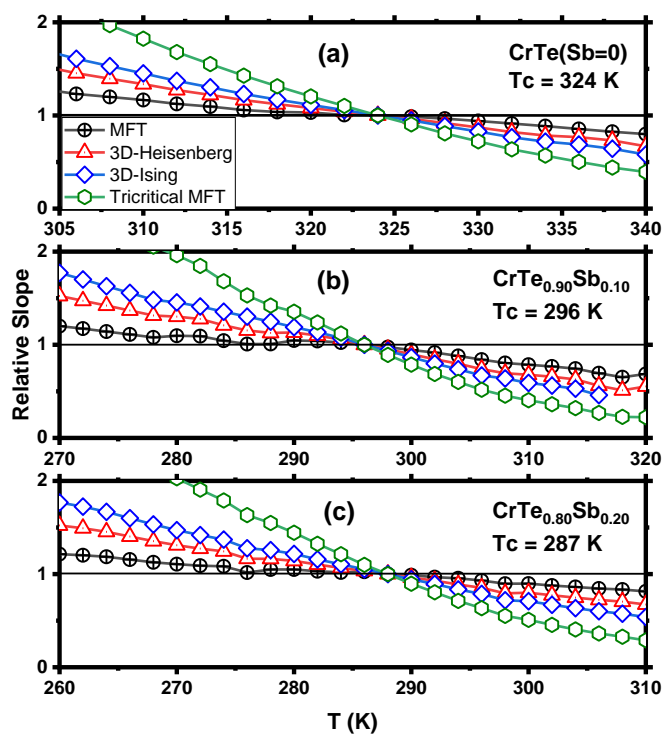


Figure 7: Variations of the relative slope (RS) with temperature for $\text{CrTe}_{1-x}\text{Sb}_x$: (a) $x=0.0$, (b) $x=0.1$ and (c) $x=0.2$ samples.

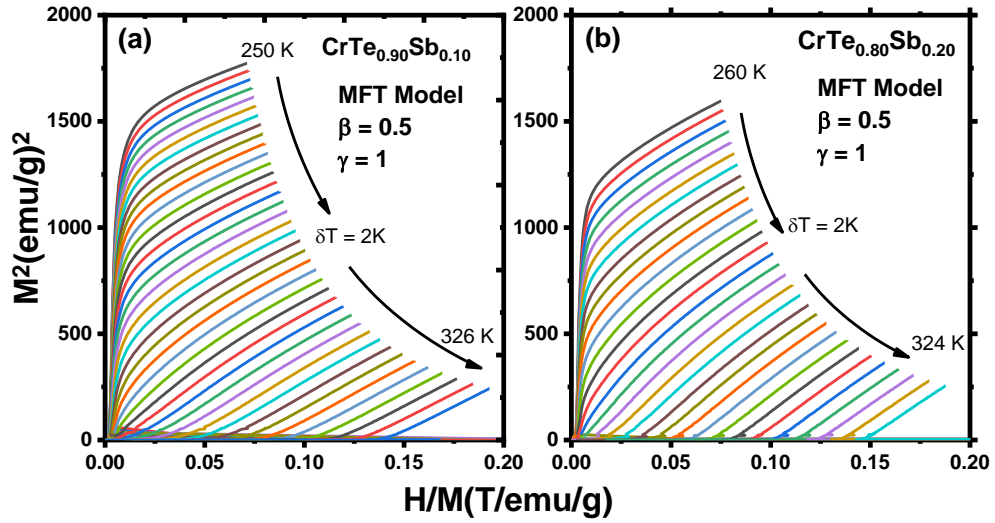


Figure 8: The Modified Arrott plots using MFT for $\text{CrTe}_{1-x}\text{Sb}_x$ ($x=0.1$ and 0.2).

The mean field representation of the modified Arrott plots (Fig. 6 and 8) have been used to extract the spontaneous magnetization $M_s(T)$ and the inverse of the magnetic susceptibility $\chi_0^{-1}(T)$. At each temperature; the curves at high fields are linearly fitted to Eq. 4 and extended to the $M^{1/\beta}$ and $(H/M)^{1/\gamma}$ axes. The intercept points represent the $M_s(T)$ and χ_0^{-1} . The variations of $M_s(T)$ and $\chi_0^{-1}(T)$ with temperature for $\text{CrTe}_{1-x}\text{Sb}_x$ samples with $x=0.0, 0.1$ and 0.2 are presented in Figs. 9a, 10a and 11a respectively, and then fitted to Eqs. 1 and 2 in order to evaluate the critical exponents β and γ along with the transition temperature T_c . The obtained values for CrTe sample are: $\beta = 0.49 \pm 0.10$, and $\gamma = 1.04 \pm 0.02$ and $T_c = 334.0 \pm 0.1$. Similarly, for $\text{CrTe}_{1-x}\text{Sb}_x$ with $x=0.1$ and 0.2 , the values are: ($\beta = 0.50 \pm 0.01, \gamma = 0.99 \pm 0.01$ and $T_c=303.3 \pm 0.1$) and ($\beta = 0.51 \pm 0.01, \gamma = 1.00 \pm 0.01$ and $T_c = 295.4 \pm 0.1$) respectively.

The Kouvel-Fisher (K-F) plots representations of the spontaneous magnetization and the susceptibility greatly improves the accuracy of modified Arrott analysis for the critical exponents.

According to the (K-F) model [41],

$$\frac{M_s(T)}{dM_s(T)/dT} = \frac{T - T_c}{\beta} \quad (5)$$

$$\frac{\chi_0^{-1}(T)}{d\chi_0^{-1}(T)/dT} = \frac{T - T_c}{\gamma} \quad (6)$$

Both equations are linear in temperature ($T - T_c$) with slopes equal to $1/\beta$ and $1/\gamma$. Figs. 9b, 10b and 11b illustrate the K-F-plot for $CrTe_{1-x}Sb_x$ samples with $x=0.0, 0.1$ and 0.2 respectively. The obtained critical exponents for $x=0.0$ are: $\beta = 0.49 \pm 0.01$ and $\gamma = 0.94 \pm 0.02$ with $T_c = 334.4 \pm 0.3$ K. We notice that β is very close to the values obtained using the modified Arrott plot while γ -value has been slightly reduced but still near the theoretical mean-field value. Similar results have been obtained for $x=0.10$ and $x=0.20$, these are shown in Fig. 10b and Fig. 11b. All values of the critical exponents extracted from MAP as well as K-F are given in Table 3. Moreover, to obtain more accurate critical exponents (β , and γ) and the critical temperature T_c , we have adopted the iterative method for the unsubstituted sample (CrTe) based on K-F method (Eqns 5 and 6). The results shows, after four rounds, that the values of the critical exponents with T_c are stable and close to the standard mean field model, namely $\beta=0.5$, and $\gamma=1$, within the uncertainty (see table 4).

The values of third critical exponent (δ) can be calculated using the Widom scaling relation: $\delta = 1 + \frac{\gamma}{\beta}$, and β and γ values obtained from MAP and K-F method [47]. The values are listed in

Table 3.

To illustrate the validity of the K-F analysis and the confidence in the obtained critical exponents and critical behavior, we used these critical exponents to re-plot the modified Arrott plots in Figure 12. The figure shows a set of nearly perfect parallel straight lines at high field ($H > 2T$), indicating that the critical exponents β and γ values obtained using K-F method for the mean field model are quite accurate choice. Moreover, the dashed lines in the Fig. 12 are a linear fitting of isothermal magnetization extrapolated near to the origin point (0,0). The obtained T_c values are 334K, 302K and 294K for $x= 0, 0.1$ and 0.2 respectively. These values are in agreement with the T_c values obtained from K-F analysis. This further indicates that the critical exponents are close agreement with the MFT critical exponents.

Equation 3 should yield a linear graph of the magnetic isotherms at ($T=T_c$) in a log-log presentation (Fig. 13) with a slope = $1/\delta$. The linear fit yields $\delta = 2.95 \pm 0.01$. The result is consistent with the one obtained from Widom's relation as shown in Table 3.

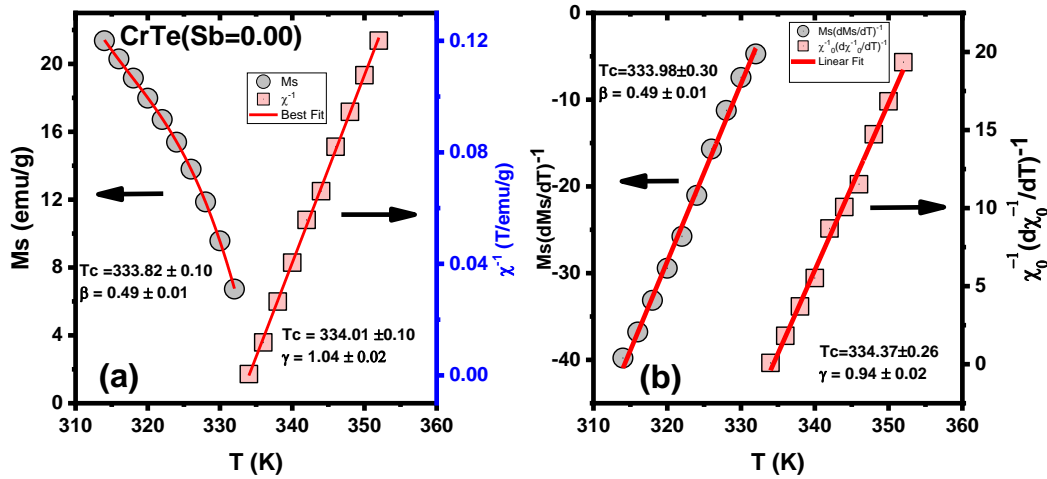


Figure 9: (a) Variations of M_s and χ_0^{-1} with temperature, (b) Kouvel-Fisher plots for $M_s(T)$ and $\chi_0^{-1}(T)$ plot for CrTe.

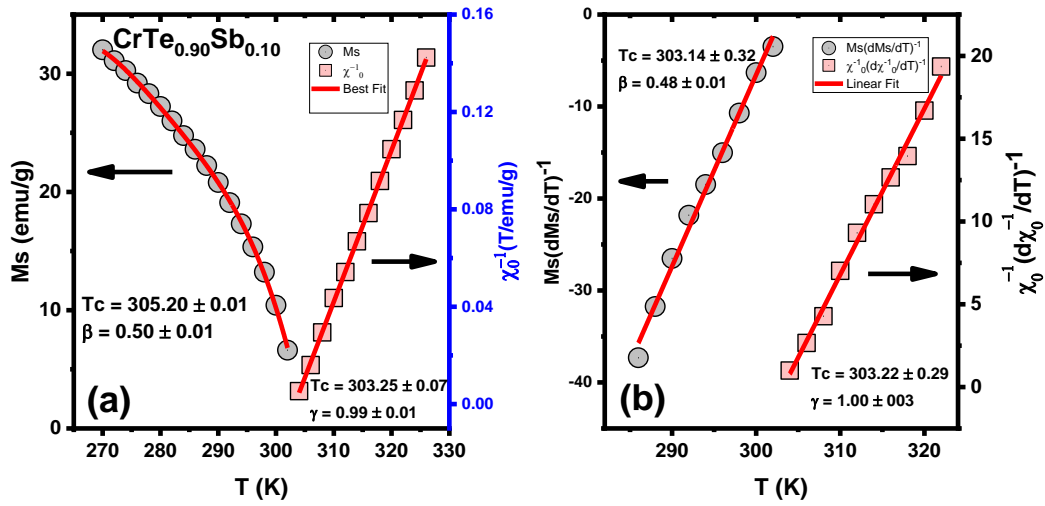


Figure 10: (a) Variations of M_s and χ_0^{-1} with temperature, (b) Kouvel-Fisher plots for $M_s(T)$ and $\chi_0^{-1}(T)$ plot for $\text{CrTe}_{0.9}\text{Sb}_{0.1}$

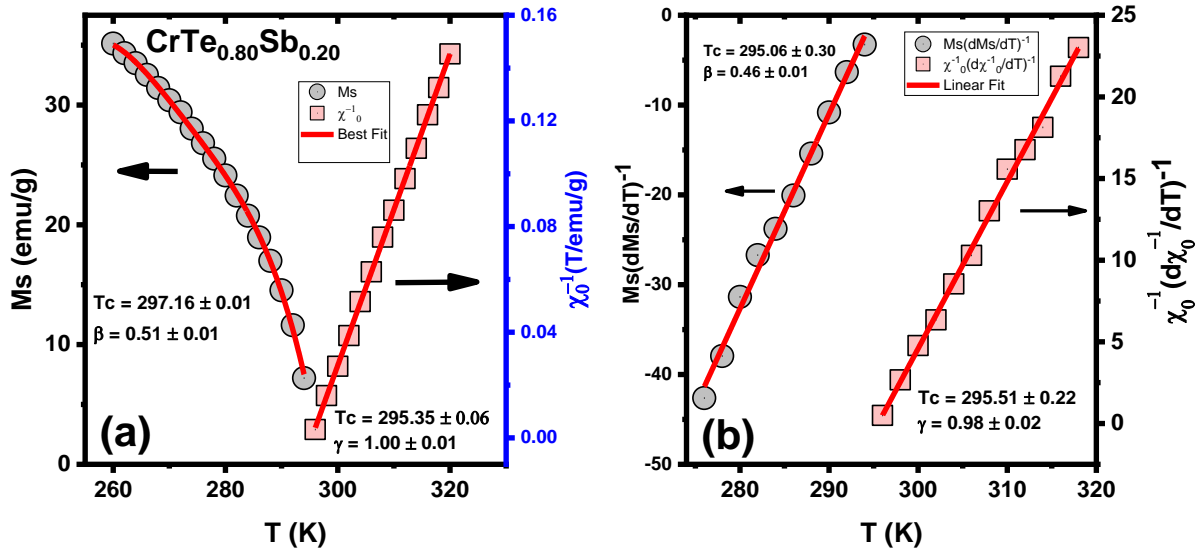


Figure 11: (a) Variations of M_s and χ_0^{-1} with temperature, (b) Kouvel-Fisher plots for $M_s(T)$ and $\chi_0^{-1}(T)$ plot for $\text{CrTe}_{0.8}\text{Sb}_{0.2}$

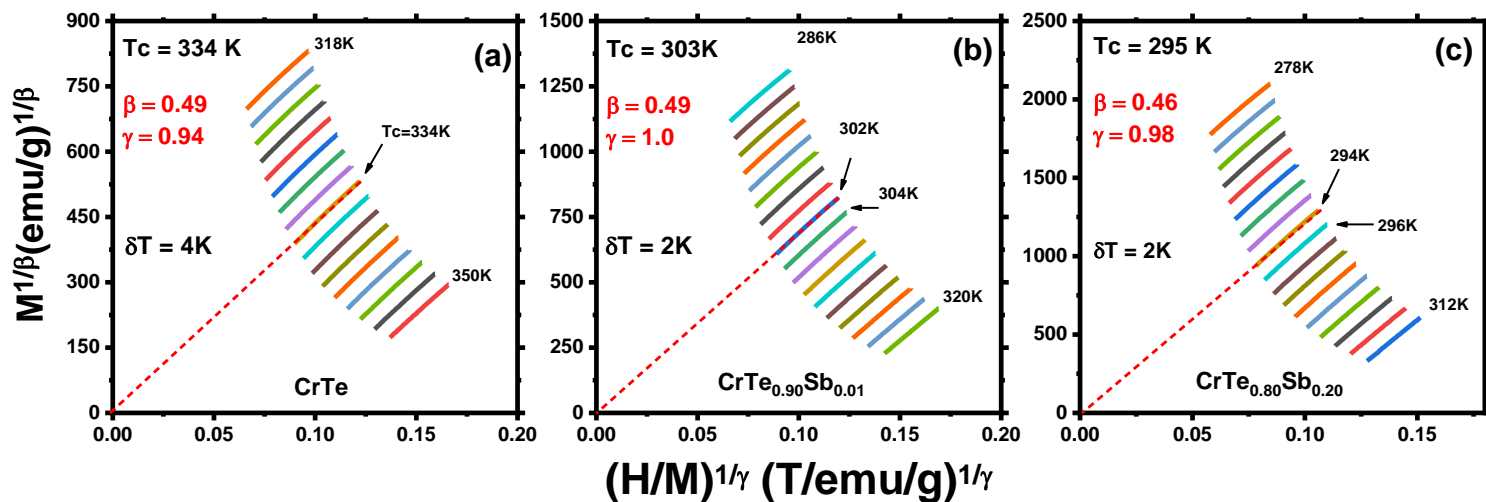


Figure 12: Modified Arrott plot of $M^{1/\beta}$ vs $(H/M)^{1/\gamma}$ at high field values with the obtained critical exponents of β and γ with a red linear dashed curve passed through the origin for. (a) CrTe, (b) CrTe_{0.90}Sb_{0.10}, and (c) CrTe_{0.80}Sb_{0.20}

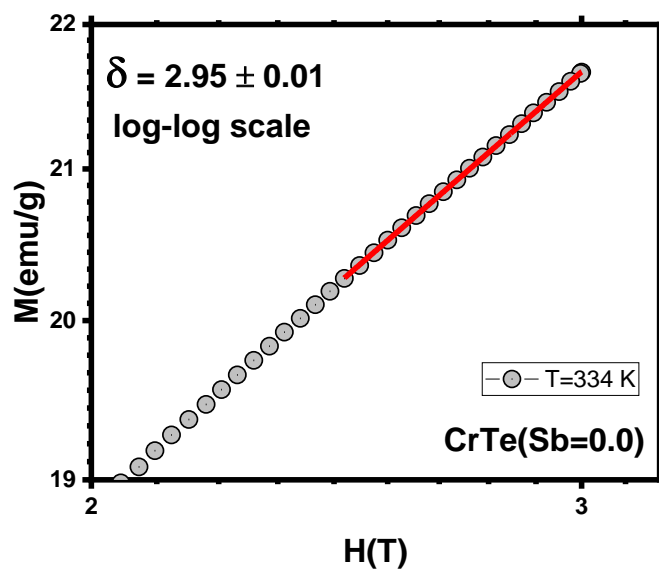


Figure 13: Critical magnetization isotherm at $T=T_c$ for CrTe in log-log scale.

Table 3: Critical exponents along with T_c for $CrTe_{1-x}Sb_x$ ($0.0 \leq x \leq 0.2$) samples.

Sample	Model	$T_c(K)$	β	γ	δ Theory	δ expt.
CrTe	MAP	334.0 ± 0.1	0.49 ± 0.01	1.04 ± 0.02	3.12 ± 0.12	2.95 ± 0.01
	K-F	334.4 ± 0.3	0.49 ± 0.01	0.94 ± 0.02	2.92 ± 0.12	
$CrTe_{0.90}Sb_{0.10}$	MAP	303.3 ± 0.1	0.50 ± 0.01	0.99 ± 0.01	2.98 ± 0.09	3.11 ± 0.01
	K-F	303.2 ± 0.3	0.48 ± 0.01	1.00 ± 0.03	3.08 ± 0.16	
$CrTe_{0.80}Sb_{0.20}$	MAP	295.4 ± 0.1	0.51 ± 0.01	1.00 ± 0.01	2.96 ± 0.09	2.90 ± 0.01
	K-F	295.5 ± 0.2	0.46 ± 0.01	0.98 ± 0.02	3.13 ± 0.13	

Table 4: Critical exponents along with T_c for CrTe sample using the iterative method

Iteration #	Initials		T_c (K)	β	γ
	β	γ			
0	0.5	1	334.37 ± 0.26	0.49 ± 0.01	0.94 ± 0.02
1	0.49	0.94	334.63 ± 0.52	0.48 ± 0.01	0.96 ± 0.03
2	0.48	0.96	333.95 ± 0.53	0.48 ± 0.01	0.97 ± 0.03
3	0.48	0.97	333.75 ± 0.54	0.48 ± 0.01	0.98 ± 0.03

Close to the transition temperature T_c , the normalized equation of state can be expressed as:

$$m = f_{\pm}(h) \quad (7)$$

Where; f_{\pm} are functions above (+) and below (-) T_c ; $m \equiv |\varepsilon|^{-\beta} M(H, \varepsilon)$ is the normalized magnetization and $h \equiv H|\varepsilon|^{-(\beta+\gamma)}$ is the normalized field.

For the correct values of the critical exponents, Eq. (7) implies that for the reliable values of β , γ and δ ; two universal branches above and below T_c presented as $M/|\varepsilon|^\beta$ vs. $H/|\varepsilon|^{(\beta+\gamma)}$ [46]. Both curves merge asymptotically at $T=T_c$. The critical exponents (β , γ and δ) obtained from Kouvel-Fisher analysis have used to represent the normalized magnetization isotherm (m) versus the normalized field (h) for all investigated samples. The scaled data for $CrTe$ sample is presented in Fig. 14 as two branches of the magnetization above and below T_c . At high fields both branches are converging towards each other at T_c . Fig. 14(b) shows the data in log-log scale, which vividly reveals the merge of the data giving further evidence for the reliability of the critical exponents' values within the mean field model. The scaling analysis has been applied for $CrTe_{1-x}Sb_x$ for $x=0.10$ and $x=0.20$. The results are shown in Fig. 15 and Fig. 16 respectively. The well-scaled data for $x=0.20$ in the current work, comparing to the scaled data published in [30] is further confirm the differences and improvements in the experiment conditions.

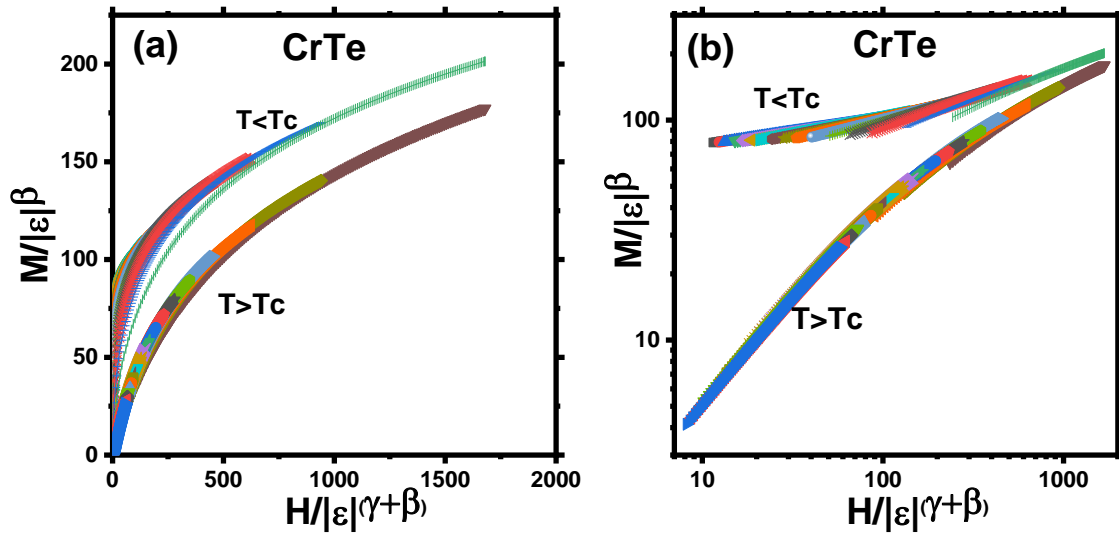


Figure 14: (a) Universal scaling behavior above and below T_c for CrTe. (b) The log-log scale representation.

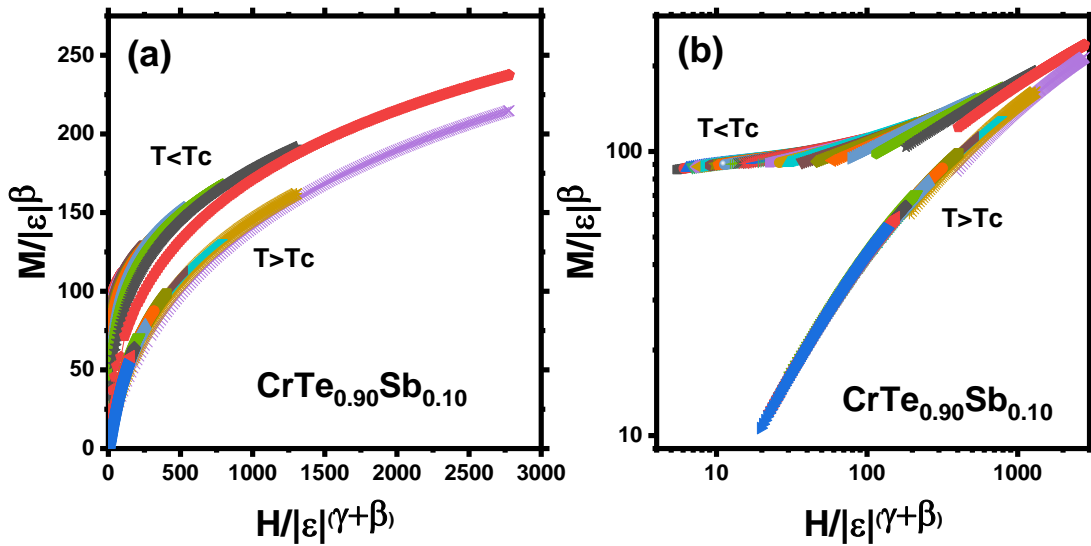


Figure 15: (a) Universal scaling behavior above and below T_c for $\text{CrTe}_{0.90}\text{Sb}_{0.10}$. (b) The log-log scale representation.

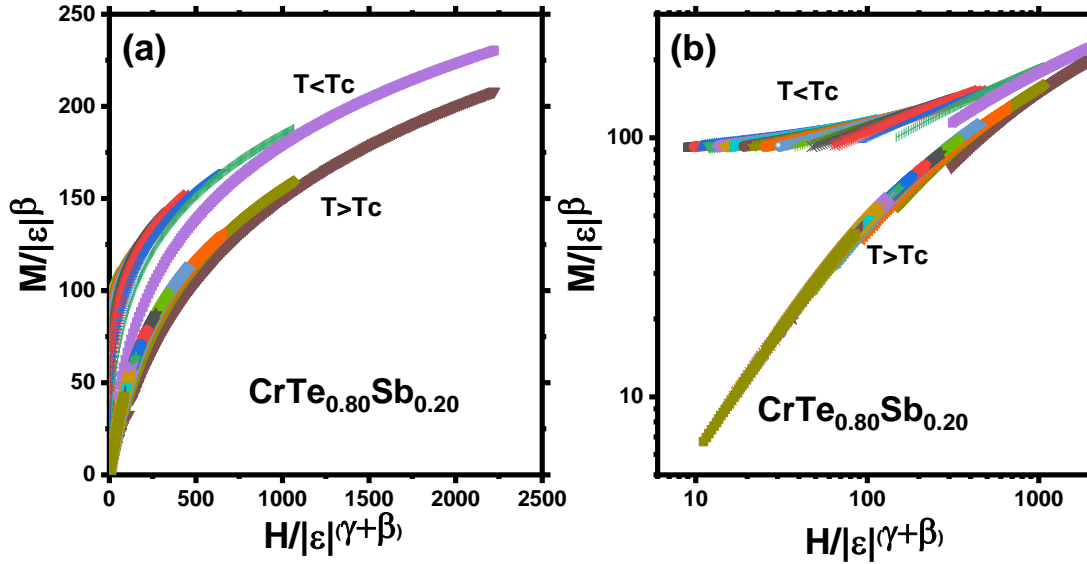


Figure 16: a) Universal scaling behavior above and below T_c for $\text{CrTe}_{0.80}\text{Sb}_{0.20}$. (b) The log-log scale representation.

Conclusion

We investigated the structural and critical behavior of $\text{CrTe}_{1-x}\text{Sb}_x$ with varying Sb contents. Antimony substitution resulted in pure NiAs -hexagonal structure with $\text{P6}_3/\text{mmc}$ (194) space-group. The critical exponents (β , γ , and δ) follow mean field model for all samples with different Sb-concentrations. The magnetization isotherms near the ferromagnetic transition follow a universal scaling behavior, giving further support for the mean field behavior in $\text{CrTe}_{1-x}\text{Sb}_x$ and confirms the obtained values of the critical exponents.

Acknowledgments

Authors from KFUPM acknowledge the support provided by the Deanship of Scientific Research at King Fahd University of Petroleum & Minerals (KFUPM) for funding this work under project

No. SR191008.

AAE acknowledges the start-up and rising stars funds by UTEP and UT-system respectively and the partial supported by the US-National Science Foundation under award **No. 2009358**.

REFERENCES

- [1] F. Lotgering, E. Gorter, Solid solutions between ferromagnetic and antiferromagnetic compounds with NiAs structure, *Journal of Physics and Chemistry of Solids*. 3 (1957) 238-249. doi:10.1016/0022-3697(57)90028-8.
- [2] M. Venkatraman, J. Neumann, The Cr-Sb (Chromium-Antimony) system, *Journal of Phase Equilibria*. 11 (1990). doi:10.1007/bf02898255.
- [3] H. Okamoto, Cr-Sb (chromium-antimony), *Journal of Phase Equilibria*. 13 (1992) 438-439. doi:10.1007/bf02674996.
- [4] H. Ipsier, K. Komarek, K. Klepp, Transition metal-chalcogen systems viii: The Cr-Te phase diagram, *Journal of the Less Common Metals*. 92 (1983) 265-282. doi:10.1016/0022-5088(83)90493-9.
- [5] H. Haraldsen, A. Neuber, Magnetochemische Untersuchungen. XXVII. Magnetische und röntgenographische Untersuchungen am System Chrom-Tellur, *Zeitschrift Für Anorganische Und Allgemeine Chemie*. 234 (1937) 353-371. doi:10.1002/zaac.19372340407.
- [6] O. Beckman and L. Lundgren, *Handbook of Magnetic Materials* (1991).
- [7] M. Akram, F. Nazar, Magnetic properties of CrTe, Cr₂₃Te₂₄, Cr₇Te₈, Cr₅Te₆, and Cr₃Te₄ compounds, *Journal of Materials Science*. 18 (1983) 423-429. doi:10.1007/bf00560631.
- [8] G. Street, E. Sawatzky, K. Lee, Magnetic properties of vapor grown crystals of hexagonal chromium telluride, *Journal of Physics and Chemistry of Solids*. 34 (1973) 1453-1455. doi:10.1016/s0022-3697(73)80048-4.
- [9] M. McGuire, V. Garlea, S. KC, V. Cooper, J. Yan, H. Cao et al., Antiferromagnetism in the van der Waals layered spin-lozenge semiconductor CrTe₃, *Physical Review B*. 95 (2017). doi:10.1103/physrevb.95.144421.
- [10] N. Grazhdankina, Magnetic First Order Phase Transitions, *Soviet Physics Uspekhi*. 11 (1969) 727-745. doi:10.1070/pu1969v011n05abeh003744.
- [11] S. Polesya, G. Kuhn, D. Benea, S. Mankovsky, H. Ebert, Electronic Structure and Magnetic Properties of Chromium Chalcogenides and Pnictides with NiAs Structure, *Zeitschrift Für Anorganische Und Allgemeine Chemie*. 639 (2013) 2826-2835. doi:10.1002/zaac.201300314.
- [12] B. Chittari, Y. Park, D. Lee, M. Han, A. MacDonald, E. Hwang et al., Electronic and magnetic properties of single-layer MPX₃ metal phosphorous trichalcogenides, *Physical Review B*. 94 (2016). doi:10.1103/physrevb.94.184428.

- [13] P. Ajayan, P. Kim, K. Banerjee, Two-dimensional van der Waals materials, *Physics Today*. 69 (2016) 38-44. doi:10.1063/pt.3.3297.
- [14] M. Hamad, E. Martinez-Teran, Y. Maswadeh, R. Hamad, E. Al-Nahari, A. El-Gendy et al., Room temperature magnetocaloric effect in CrTe_{1-x}Sb_x alloys, *Journal of Magnetism And Magnetic Materials*. 514 (2020) 167171. doi:10.1016/j.jmmm.2020.167171.
- [15] L. Zhang, X. He, A. Zhang, Q. Xiao, W. Lu, F. Chen et al., Tunable Curie temperature in layered ferromagnetic Cr_{5+x}Te₈ single crystals, *APL Materials*. 8 (2020) 031101. doi:10.1063/1.5143387.
- [16] A. Andresen, E. Zeppezauer, T. Boive, B. Nordström, C. Brändén, The Magnetic Structure of Cr₂Te₃, Cr₃Te₄, and Cr₅Te₆., *Acta Chemica Scandinavica*. 24 (1970) 3495-3509. doi:10.3891/acta.chem.scand.24-3495.
- [17] M. Chevreton, E. Bertaut, F. Jellinek, Quelques remarques sur le système Cr–Te, *Acta Crystallographica*. 16 (1963) 431-431. doi:10.1107/s0365110x63001134.
- [18] A. Andresen, E. Zeppezauer, T. Boive, B. Nordström, C. Brändén, The Magnetic Structure of Cr₂Te₃, Cr₃Te₄, and Cr₅Te₆., *Acta Chemica Scandinavica*. 24 (1970) 3495-3509. doi:10.3891/acta.chem.scand.24-3495.
- [19] Goodenough J B 1963 *Magnetism and the Chemical Bond* (New York: Interscience).
- [20] G. Bhimanapati, Z. Lin, V. Meunier, Y. Jung, J. Cha, S. Das et al., Recent Advances in Two-Dimensional Materials beyond Graphene, *ACS Nano*. 9 (2015) 11509-11539. doi:10.1021/acsnano.5b05556.
- [21] N. Suzuki, T. Kanomata, R. Konno, T. Kaneko, H. Yamauchi, K. Koyama et al., Magnetic phase diagram of CrTe_{1-x}Sb_x (0.0≤x≤1.0), *Journal Of Alloys And Compounds*. 290 (1999) 25-29. doi:10.1016/s0925-8388(99)00244-3.
- [22] T. Hirone, S. Maeda, I. Tsubokawa, N. Tsuya, On the Magnetic Properties of the System MnSb–CrSb, *Journal of the Physical Society of Japan*. 11 (1956) 1083-1087. doi:10.1143/jpsj.11.1083.
- [23] A. Snow, Magnetic Moment Orientation and Thermal Expansion of Antiferromagnetic CrSb, *Reviews of Modern Physics*. 25 (1953) 127-127. doi:10.1103/revmodphys.25.127.
- [24] A. Snow, Neutron Diffraction Investigation of the Atomic Magnetic Moment Orientation in the Antiferromagnetic Compound CrSb, *Physical Review*. 85 (1952) 365-365. doi:10.1103/physrev.85.365.
- [25] W. Takei, D. Cox, G. Shirane, Magnetic Structures in the MnSb–CrSb System, *Physical Review*. 129 (1963) 2008-2018. doi:10.1103/physrev.129.2008.
- [26] N. P. Grazhdankina, L. G. Gaidukov, K. P. Rodionov, M. I. Oleinik, and V. A. Shchipanov, *J. Exptl. Theoret. Phys. (U.S.S.R.)* 40, 433-440 (February, 1961)
- [27] W. Takei, D. Cox, G. Shirane, Magnetic Structures in CrTe—CrSb Solid Solutions, *Journal of Applied Physics*. 37 (1966) 973-974. doi:10.1063/1.1708545.

- [28] Grazhdankina N P and Zaynullina R I, *Zh. Eksp. Teor. Fiz.* 59 1896 (1970) (Engl. Trans. *Sou. Phys.-JETP* 32 1025 (1971)).
- [29] P. de Gennes, Effects of Double Exchange in Magnetic Crystals, *Physical Review*. 118 (1960) 141-154. doi:10.1103/physrev.118.141.
- [30] M. Hamad, K. Ziq, Critical behavior of CrTe_{1-x}Sb_x ferromagnet, *AIP Advances*. 8 (2018) 101416. doi:10.1063/1.5042550.
- [31] A. West, *Solid State Chemistry and Its Applications*, 2nd ed. (Wiley, Chichester, West Sussex, UK, 2014), p. 187.
- [32] M. Hamad, I. Abdel-Latif, K. Ziq, Effect of cobalt doping in Nd_{1-x}Sr_xMn_{1-y}Co_yO₃, *Journal of Physics: Conference Series*. 869 (2017) 012032. doi:10.1088/1742-6596/869/1/012032.
- [33] L. Elton, D. Jackson, X-Ray Diffraction and the Bragg Law, *American Journal of Physics*. 34 (1966) 1036-1038. doi:10.1119/1.1972439.
- [34] H. Rietveld, The Rietveld method, *Physica Scripta*. 89 (2014) 098002. doi:10.1088/0031-8949/89/9/098002.
- [35] K. El-Sayed, Z. Heiba, Quantitative phase analysis from X-ray powder diffraction data using a two-stage method, *Powder Diffraction*. 9 (1994) 246-249. doi:10.1017/s0885715600018959.
- [36] H. Harladsen, Die Phasenverhältnisse im System Chrom-Schwefel, *Zeitschrift Für Anorganische Und Allgemeine Chemie*. 234 (1937) 372-390. doi:10.1002/zaac.19372340408.
- [37] T. Kong, K. Stolze, D. Ni, S. Kushwaha, R. Cava, Anisotropic magnetic properties of the ferromagnetic semiconductor CrSbSe₃, *Physical Review Materials*. 2 (2018). doi:10.1103/physrevmaterials.2.014410.
- [38] M. Hamad, PhD thesis, "Developing Near Room Temperature Magnetocaloric Materials", King Fahd University of Petroleum and Minerals, (2018). <http://eprints.kfupm.edu.sa/140778/>
- [39] M. Hamad, Y. Maswadeh, K. Ziq, Effects of Ni substitutions on the critical behaviors in Nd_{0.6}Sr_{0.4}Mn_{1-x}Ni_xO₃ manganite, *Journal of Magnetism And Magnetic Materials*. 491 (2019) 165609. doi:10.1016/j.jmmm.2019.165609.
- [40] A. Arrott, Criterion for Ferromagnetism from Observations of Magnetic Isotherms, *Physical Review*. 108 (1957) 1394-1396. doi:10.1103/physrev.108.1394.
- [41] J. Kouvel, M. Fisher, Detailed Magnetic Behavior of Nickel Near its Curie Point, *Physical Review*. 136 (1964) A1626-A1632. doi:10.1103/physrev.136.a1626.
- [42] H. E. Stanley, *Introduction to Phase Transitions and Critical Phenomena* (Oxford U. P., London and New York, 1971).
- [43] J. Kouvel, M. Fisher, Detailed Magnetic Behavior of Nickel Near its Curie Point, *Physical Review*. 136 (1964) A1626-A1632. doi:10.1103/physrev.136.a1626.
- [44] A. Arrott, J. Noakes, Approximate Equation of State For Nickel Near its Critical Temperature, *Physical Review Letters*. 19 (1967) 786-789. doi:10.1103/physrevlett.19.786.

[45] B. Banerjee, On a generalised approach to first and second order magnetic transitions, *Physics Letters*. 12 (1964) 16-17. doi:10.1016/0031-9163(64)91158-8.

[46] J. Fan, L. Ling, B. Hong, L. Zhang, L. Pi, Y. Zhang, Critical properties of the perovskite manganite $\text{La}_{0.1}\text{Nd}_{0.6}\text{Sr}_{0.3}\text{MnO}_3$, *Physical Review B*. 81 (2010). doi:10.1103/physrevb.81.144426.

[47] B. Widom, Degree of the Critical Isotherm, *The Journal of Chemical Physics*. 41 (1964) 1633-1634. doi:10.1063/1.1726135.